BEAM DIAGNOSTICS AND RADIATION DETECTION SYSTEM

1. Introduction

Particle accelerators are the main tool in high-energy physics. In addition, a large number of synchrotron radiation sources and free electron lasers are operating and under construction in the world. Particle accelerators are also used in industry and for medical purposes. Very high requirements are imposed on the quality of beams in modern accelerators; therefore, the efficient operation of accelerator facilities is practically inconceivable without accurate and reliable systems for beam diagnostics, which provide the possibility of regular tuning of the accelerator parameters based on the measurement results [1-7].

Efforts to achieve the beam with small sizes are ongoing. Collider luminosity is directly dependent on cross beam size at the interaction point, therefore, measuring and controlling a small beam size (<< 1 um) is critical to collider experiments. Free electron lasers (FELs) also require a high brightness beam. In the plasma-based accelerator, the beam size should be in the range less than millimeters [8-14]. A compact electron accelerator whose structure is a femtosecond laser pulse (dielectric laser accelerator), excited dielectric microstructure requires a sub-um beam size measurements. Therefore, measuring a beam with a micrometer size is an important task in accelerator physics [15-20].

The beam diagnostics can be considered in a transverse (spatial) and longitudinal (temporal) directions. The methods and associated apparatus for these diagnostics are sometimes similar but have certain differences for particular cases [21-40]. Here we will consider the most common transverse and longitudinal diagnostics methods. For more details, readers advised to follow references at the bottom of the article.

2. Transverse beam diagnostics

2.1 Luminescent screens

The simplest and most accessible means of visual observation of a particle beam is a luminescent screen (phosphor screen) placed in the path of the beam [41-43]. A phosphor screen is a plate (usually aluminum) with a layer of phosphor deposited on it - a substance that emits photons of visible light when beam particles hit it. Interacting with the phosphor substance, the beam particles lose part of their energy for ionization, and, in turn a part of the ionization losses is converted into optical radiation. The radiation process takes place in three stages: 1) absorption of the energy of the beam particles by the atoms of the substance; 2) transfer of a part of the absorbed energy to the luminescence centers with their excitation to the emitting state; 3) return of luminescence centers to the ground state with emission of photons. The mechanisms of luminescence at the molecular level in different luminophores are different.

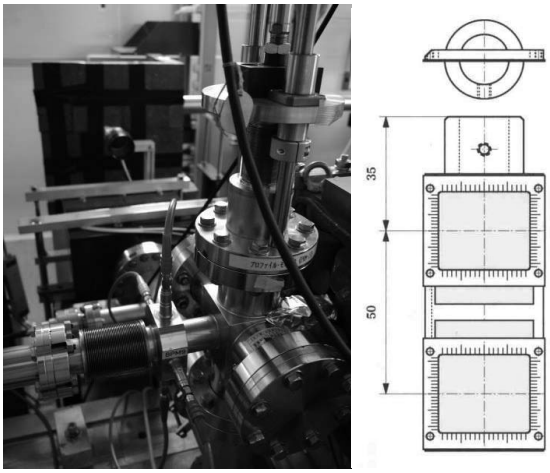

Fig. 1. Typical screen monitor vacuum chamber and a screen holder.

A photograph of a phosphor screen in a vacuum chamber is shown in Fig. 1. The screen is introduced into the vacuum chamber using a remotely controlled drive, the image of the beam on the screen is recorded by a CCD camera (Fig. 2).

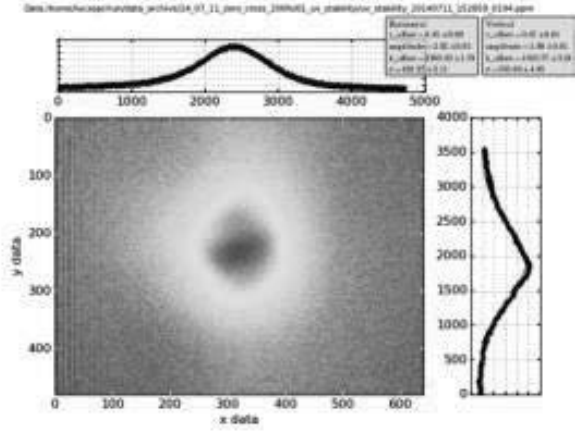

Fig.2. Typical CCD image of the electron beam

The coordinate grid applied either to the surface of the screen or to the screen holder makes it possible to determine the position of the center of mass of the beam and its shape. Having measured for a specific sensor and camera the experimental dependence of the spot size displayed on the screen on the value of the beam current, it is possible to determine the root-mean-square dimensions of the beam in the vertical and horizontal planes using the coordinate grid with satisfactory accuracy. The sensitivity of such a sensor is high, reaching 10^7 particles/cm^2 even with the traditional coating of the screen with a layer of zinc sulfide ZnS. Many laboratories are intensively developing materials with a high light yield, high linearity of the light characteristic, good spatial resolution, and radiation resistance.

The most common materials used for the manufacture of a phosphor screens are the following:

1. Powder phosphors. The resolution of such a phosphor is limited by the average grain size and usually amounts to several tens of microns. Such screens are economical and versatile due to their simple manufacturing process. For measurements with a high temporal resolution, compositions with an emission time of no more than 45 ps have been developed.
2. Ceramic phosphors. Ceramic phosphor screens are made by sintering a luminescent powder, usually aluminum oxide Al2O3, doped with chromium (Chromax). This material has a 20-30 times higher light yield compared to zinc sulfide (300-400 photons per one high-energy particle) and has good linearity up to densities of the order of 10^{14} particles/cm2. Cerium-doped yttrium-aluminum garnet (YAG: Ce), boron nitride BN, which has better thermal stability, and zirconium oxide ZrO2 are also quite often used [22]. Screen sizes and thicknesses are usually selected based on operational requirements. Since the phosphor grains are linked together, the spatial resolution is determined by the size of several grains and is of the order of 100 μm.
3. Monocrystalline scintillators. Translucent cerium-doped yttrium-aluminum garnet single crystals were proposed for beam diagnostics about 30 years ago, but their use was limited by their high cost. Recently, a large number of YAG crystals are being manufactured for the laser industry, and therefore their cost has dropped significantly. Monocrystalline scintillators have a number of advantages over powder and ceramic phosphors. They are effective in high vacuum conditions, have good light output, are radiation resistant, emit in a narrow spectral range, which reduces chromatic aberration. The main advantage of single crystal scintillators is their high

spatial resolution. In the case of YAG crystals, a resolution of 40 μm for high-density beams and 10 μm for low-density beams was achieved. Specially manufactured YAG crystals with a thin (several micrometers) surface layer doped with cerium provide a resolution of about 1 μm. The spatial resolution of single-crystal scintillators is limited by the saturation effect that occurs at beam densities exceeding 10^{13} particles/cm2 and leads to spreading of the light spot. Luminophores with good linearity open up the possibility of diagnosing beams with transverse dimensions of the order of 0.1 mm using linear optics with high magnification and projecting an enlarged image of the beam onto the input of a digital camera system. Subsequent data processing, taking into account nonlinearities in the measuring system, makes it possible to obtain the particle density distribution over any beam cross section with a spatial resolution of tens of micrometers.

The main disadvantage of phosphor screens is their opacity for the beam. Intensive use of phosphor screens for diagnostics of beams, especially proton and ion beams, leads to a rather rapid damage to the screens due to pulsed thermal and electrical loads. Therefore, the choice of material and design of a modern phosphor screen is a non-trivial task. In addition, the camera, the lens system and the window for light output from the vacuum chamber are exposed to radiation. Glass lenses and light windows darken when exposed to radiation and must be replaced after a certain period of use. Quartz windows are more stable.

Luminescent screens traditionally used in beam transport lines and beam injectors. If there is a significant coupling coefficient of betatron oscillations or the presence of dispersion in combination with a large energy spread of the beam, the phase ellipse rotates in the coordinate space x, y during transportation along the line. In this case, observing the evolution of the beam image on the screens installed along the line, one can obtain necessary information for injection tuning.

2.2 Wire scanner

To measure the transverse distribution of the beam density in particle accelerators, sensors with a moving wire (wire scanner) is used, see for instance [44, 45]. In such a sensor, thin, 5-10um tungsten or carbon wire moves in the transverse direction, crossing the beam path. The bremsstrahlung radiation intensity proportional to the intrinsic amount of charged particles interacting with the wire is detected downstream of the scanner.

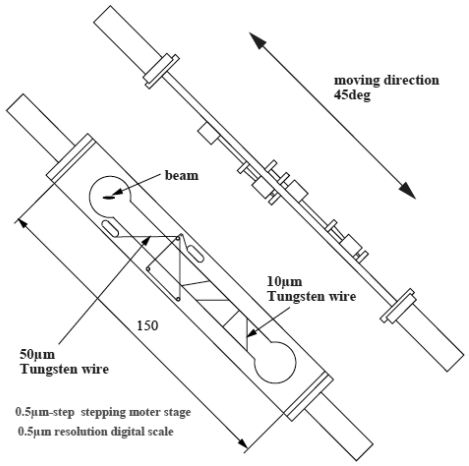

Fig.3 Wire mount in the wire scanner chamber

The scanner design is shown in Fig. 3. Three wires for horizontal, vertical and 45 degree projection, allow measurements of beam density.

Figure 4 shows a graph of the dependence of the position of the wire. Scanning speed is limited by the backlash and inertia of the moving parts of the drive. The drive motor

operates in the atmosphere, the drive mechanism in vacuum. The most complex element of such sensors is the drive mechanism, since very high requirements are imposed on it both in terms of the linearity of the wire movement, which determines accuracy, and in terms of reliability when working in a vacuum.

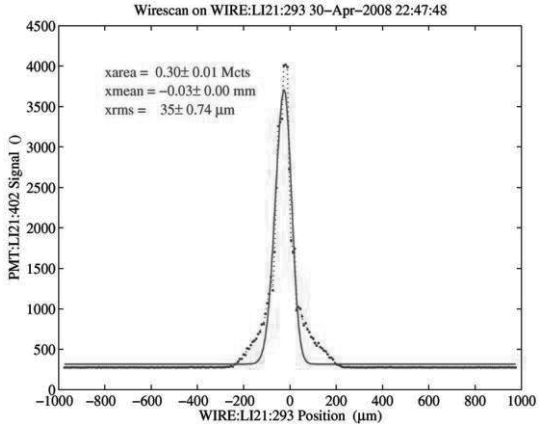

Fig.4: Example of scanned beam profile.

2.3 Transition radiation

Despite the convenience of phosphor screens, their use for diagnostics of beams with transverse sizes of less than 100 um is practically impossible due to the spreading of the light spot. For diagnostics of such beams, sensors based on transition radiation are being developed [46,47], the spatial resolution of which is limited only by the diffraction limit. In addition, the angular distribution of transition radiation depends on the energy and emittance of the beam, which makes it possible to use it for measuring of these values.

A charged particle, moving through a medium that is inhomogeneous in terms of electromagnetic properties, emits photons, as predicted by I.M. Frank and V.L. Ginzburg [48] back in 1945. Transition radiation is generated when particles passes through a boundary between matters with different dielectric constants. Similar radiation appear when a charge particle moves in a conducting chamber of variable cross-section, for example, through a hole in a foil or through a collimator. In this case radiation is refer to as Diffraction Radiation. Radiation is directed to the upper and lower hemispheres relative to the boundary of two media and, for relativistic particles, is concentrated in narrow cones with an opening angle of 1/γ, where γ is the Lorentz factor.

Using the formalism developed in [49], the distribution of the intensity of the transition radiation of a single relativistic electron (γ ≫ 1) over the horizontal θ and vertical ϕ angles can be written as:

$$\frac{dW}{d\omega d\Omega} = \frac{e^2\beta^2}{\pi^2 c}\cos^2\psi\left[\frac{\sin\theta - \beta\cos\phi\sin\psi}{(1-\beta\sin\theta\cos\phi\sin\psi)^2 - \beta^2\cos^2\theta\cos^2\psi}\right]^2$$

where ψ is the angle between the direction of motion of the particle and the plane of the boundary of the two media. In Fig. 5 an example of the angular distribution of the transition radiation for a different electron energies is shown.

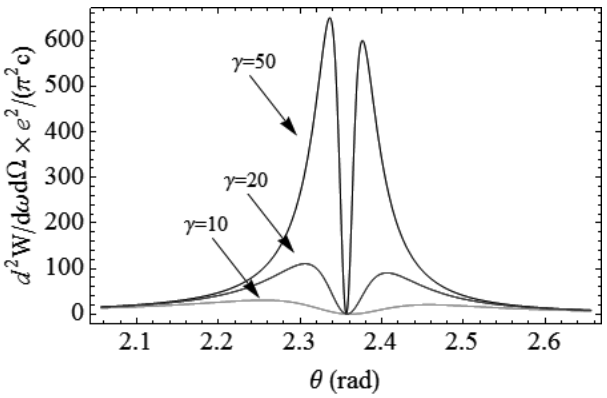

Fig. 5 TR angular distribution

In reality, electron beam consist of a large number of electrons emitting such a two-lobe distributed intensity profile. That is why for electron beam sizes greater than 50um one can always observe smooth 2D Gaussian-like intensity distribution. A typical OTR image is shown at Fig. 6.

Fig. 6 Typical OTR image

The resolution in this case is determined by the diffraction limit of the focusing optics used along with CCD camera for the image acquisition.

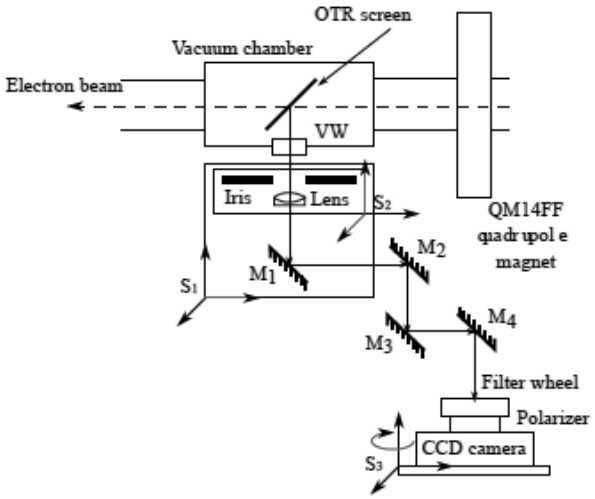

Fig. 7 A schematic of the OTR setup

The diagram of a OTR setup is shown in Fig.7. A metal foil is placed in a vacuum chamber at an angle of 45 ° to the beam trajectory so that the radiation is directed perpendicular to the chamber axis. The extracted radiation is recorded by a digital CCD camera and then processed in the control computer according to the following algorithm. First, the center of the three-dimensional angular distribution is determined, then two-dimensional sections are selected near the center in the horizontal and vertical directions. Fitting experimental data the calculated curve gives the value of the angular divergence and beam energy. Examples of beam images and fitting results are shown in Fig. 8 [26].

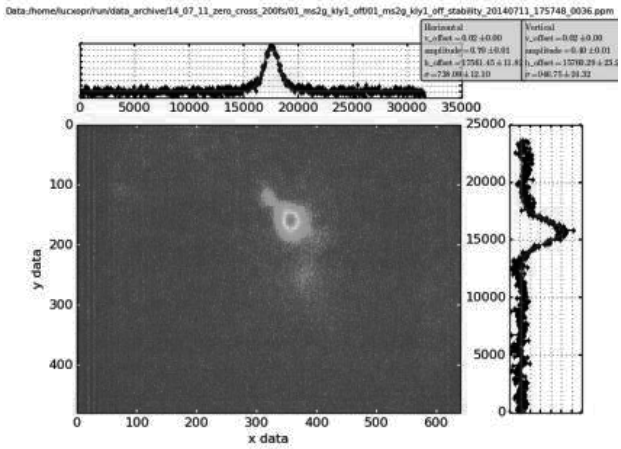

Fig. 8 Typical OTR image and projected beam profiles

Recently, the OTR-based diagnostics was extended beyond diffraction limit and the 1um resolution was demonstrated [50, 51].

3. Longitudinal diagnostics

Over the last decade, with the construction of modern accelerators, the longitudinal diagnostics of charged particles beams become an important topic [52-60]. Nowadays, the well-established methods based on RF deflecting cavities, streak cameras and electro-optics methods. Although recent advances in these directions provide promising results, reliable methods of the femtosecond electron bunch length determination still need to be developed. The streak camera can provide a temporal resolution of about 300 fs. RF deflecting cavities provide the required resolution, but the changes of the accelerator high-power RF distribution is required. In addition, such equipment requires significant beamline space allocation for equipment installation. The electro-optic method requires fs laser source and careful calibration [61-62].

Another promised technique for the longitudinal bunch profile reconstruction are based on the measurement of coherent radiation spectrum. The polarization radiation in this case is usually chosen. That includes

coherent transition and diffraction radiations, coherent Smith-Purcell and Cherenkov radiations. The common problem is the correct spectra acquisition and data post-processing.

3.1 Michaelson interferometer

Michaelson interferometer (MI) is the most common configuration for optical interference measurements. It can be extended to the long wavelength range covering THz and IR [16, 24]. Interferometer design is much simpler than that of the so-called Martin-Puplett interferometers [25, 26, 27, 28], as it requires only one detector and does not use wire grid polarizers. MI also works without any special alignment techniques. It significantly increases the quality of the measurements. Figure 9 shows a general MI layout for THz spectral range.

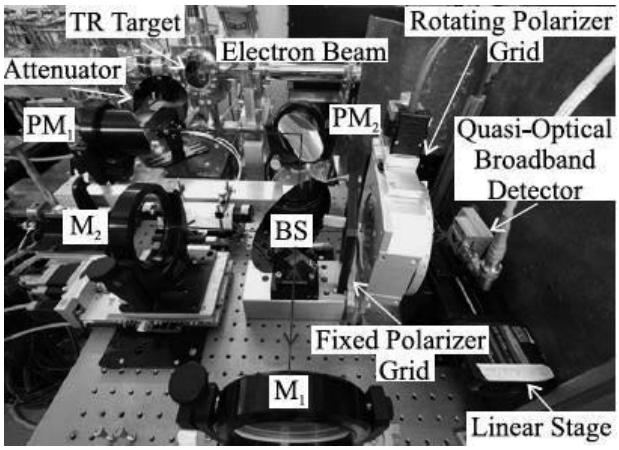

Fig.9 General layout of Michaelson interferometer and THz emission transport line.

The interference pattern is produced by splitting the incoming radiation into two paths, reflecting and recombining them through the splitter again. The setup consisted of a THz radiation transport line, beam splitter (BS), two flat aluminum mirrors (movable M1 and fixed M2 mirrors), an alignment system, THz polarizer, and a detector.

The BS is installed at the center of the interferometer at 45 degree with respect to the incoming radiation. To obtain the autocorrelation dependency (interferogram), the M2 is moved back and forth along the optical axis.

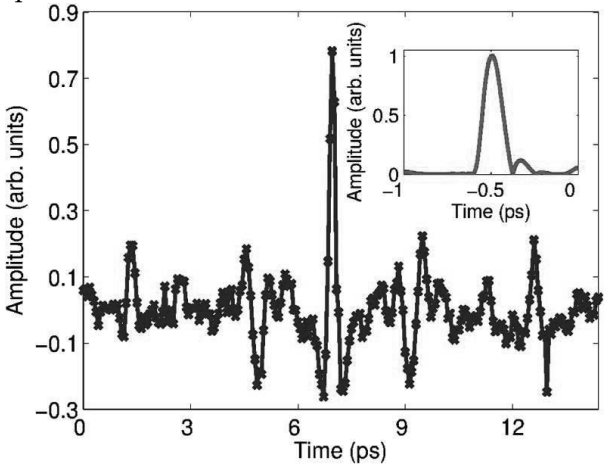

Fig.10 Interferogram obtained with Michelson interferometer. The inset shows reconstructed bunch longitudinal profile.

3.1.1 MI beam splitter

The beam splitter determines the quality of the interferogram. PET or Si beam splitters are now widely used in MIs. The Mylar type is commercially available. Mylar splitters generally used to study a wide spectrum where the efficiency of PET beam splitters is strongly dependent on splitter thickness and emission wavelength. Silicon splitters have recently been found to be much more efficient than PET splitters in the terahertz region. The beam splitter's reflectance and transmission vary according to the incidental angle, index of refraction, and thickness.

3.1.2 MI mirror motion system

The MI motion system directly affects the quality of the spectral measurements. The system should have sufficient mechanical

resolution, stability, repeatability, and compatibility with modern hardware and software controllers. It should also be calibrated and its linearity should be checked for high accuracy.

To evaluate the mechanical resolution and travel range of the operating system required by an MI for the measurement of constant frequency spectra, one should consider the target spectral resolution and emission spectral bandwidth. In order to determine the radiation spectrum in the range of 0.1-4 THz by 10 GHz resolution, it needs to consider the operating system with a resolution of 19.2 μm, and the minimum travel range of 15 mm.

3.1.3 Detectors for THz spectroscopy

To choose an appropriate detector for the microwave spectroscopy based longitudinal beam diagnostics, one should understand the present status and commercial availability of the detection systems. Practical detector devices falling into the broad groups of thermal, rectifying and photoconductive types. More exact information can be found in a number of excellent reviews of millimeter-submillimetre detectors which have been given by several authors such as [63,64].

The submillimetre region lies between the microwave region and that part of the far infrared around 10 um wavelength. The usual detection systems respond to only one mode of the radiation field and, for the best sensitivity, heterodyne receivers are often used. The ultimate limit to detector performance is provided by signal fluctuations, which in most cases can be described as thermal in origin.

As a general rule, coherent detectors are more useful at the longer infrared wavelengths and for experiments requiring narrow infrared bandwidths. From the other hand, incoherent detectors are favored for short-wavelength, broadband measurements. The infrared portion of the electromagnetic spectrum is a crossover region where the eventual choice between coherent and incoherent detectors is dictated by the application requirements such as spectral range, spectral resolution, and spatial resolution.

Except for devices using photocathodes, electron multiplication and some of rectifiers, all incoherent infrared detectors presently in use (photoconductors, photovoltaic devices, and bolometers) make use of sophisticated electronic circuitry to measure very weak currents or voltages produced in the device. This is always restricts the speed of response of these detectors.

The sensitivity of direct detectors is often measured in terms of the noise equivalent power (NEP). The smaller the NEP, the more sensitive the detector. The NEP of a detector is directly related to the minimum number of photons at a particular wavelength that can be detected in 1 sec.

In addition to the NEP, many other characteristics must be considered in the selection of a receiver for real observations. These characteristics are not usually independent parameters, so detector performance must be optimised in accordance to the application. References in which the general principles of infrared detection are discussed include [65-68].

In most spectroscopic measurements being made interferometrically, most commonly by the multiplex method of Fourier-transform spectrometry. This has generally favored the development of detectors operating over large spectral ranges, with quite large etendue and with emphasis often placed on good sensitivity rather than convenience, ruggedness or fast

response time. Such detectors have also been used with coherent sources. Detector devices of the rectifier type are single-mode devices although they do not generally offer any improvement in sensitivity, but are usually employed for their high speed of response. Many of the most popular IR and THz detectors are available commercially. Many types and variations of detector device have been considered and investigated, although only a relatively small number have achieved widespread use.

3.1.4 Schottky barrier diode detector

Schottky diode detectors are rectifier detectors with a long history of applications for electromagnetic radiation detection in the millimeter-THz-wave range. A typical Schottky detector consists of a metal contact layer deposited in a lightly doped semiconductor material grown on a heavily doped command board [43]. Response times for these devices are inherently short, as the use of the majority carrier current flow by the device removes the recovery time associated with minority carrier injections. The sensitivity of the device remains almost unchanged over the entire frequency band. It results in a slightly flat frequency response.

4. Conclusion

The purpose of article is to give the reader an opportunity to form a brief general understanding of modern means and methods of diagnostics of charged particle beams in accelerators. The reader can find more detailed information on specific issues in the works, references to which are given in the list of references.

Beam diagnostics is one of the most dynamically developing areas of accelerator physics. The latest information on the problems, achievements and trends in the further development of beam diagnostics is published in the materials of specialized international conferences: Beam Instrumentation Workshop (BIW) and Beam Diagnostics and Instrumentation for Particle Accelerators (DIPAC), as well as in the materials of the European Accelerator Conferences (EPAC), American (PAC), Asian (APAC) and Russian (RuPAC). Proceedings of the above conferences are presented on the JACoW web portal (http://www.jacow.org).

References

[1] C. Lejeune and J. Aubert, “Emittance and Brightness, definitions and measurements”, Adv. Electron. Electron Phys.,Suppl. A 13, 159 (1980).

[2] O.R. Sander, “Transverse Emiitance: Its Definition, Applications, and Measurements” in “Accelerator Instrumentation”, E. R. Beadle and V. J. Castillo, edts., (AIP CP212, 1991) pp. 127-155.

[3] R. Becker and W.B. Herrmannsfeldt, “Why pi and why mrad”, Rev. Sci. Instrum. 77(2006).

[4] A. Wu Chao, M. Tigner “Handbook of Accelerator Handbook of Accelerator Physics and Engineering Physics and Engineering” World Scientific, 2013

[5] C. A. Brau “What Brightness means” in The Physics and Applications of High Brightness Electron Beam”, World Scientific, 2003

[6] M. Reiser, “Theory and design of charged particle beams” , Wiley, 1994

[7] Shyh - Yuan Lee, “Accelerator Physics” , World Scientific, 2018

[8] J. Clarke “The Science and Technology of Undulators and Wiggles” Oxford Science Publications, 2004

[9] H. Loos, “Diagnostic Systems for High Brightness Electron Injectors”, talk at 48thICFA Advanced Beam Dynamics Workshop on Future Light Sources, SLAC 2010

[10] B.E.Carsten et al., ” Measuring emittance of nonthermalized electron beams from photoinjectors” Nuclear Instruments and Methods in Physics Research A 331 (1993) 791-796

[11] K.T. McDonald and D.P.Russel “Methods of emittance measurememnts”, Frontiers of Particle Beams Observation Diagnosis and Correction (1988), Volume: 08544, pp.1-12

[12] M.P. Stockli “Measuring and Analyzing Transverse Emittances of Charged Particle Beams”, talk at BIW’06, Fermi National Accelerator Laboratory, Batavia, IL, May 1, 2006

[13] C.P. Welsch “Low energy beam diagnostics developments within DITANET”, Proceedings of 2011 Particle Accelerator Conference, New York, NY, USA, MOP186

[14] M. Minty, F. Zimmermann, “Measurement and control of charged particle beams”, Springer (2003)

[15] P. Emma, A. Brachmann, D. Dowell, et al., “Beam brightness measurements in the LCLS Injector”, Compact X-RAY FELs using High-Brightness Beams, Aug.5-6, 2010, LBNL

[16] A. H. Lumpkin et al. “High-brightness beam diagnostics for the APS linac”, Proceedings of the 1999 Particle Accelerator Conference, New York, 1999, pp.2134-2136

[17] N.Terunuma “KEK ATF beam instrumentation program”, Proceedings of 2011 Particle Accelerator Conference, New York, NY, USA, WEODN2

[18] J. Frisch et al.,“Beam measurements at LCLS”, BIW08, MOIOTIO02

[19] R. Boni et al., “Activities on high brightness photo-injectors at the Frascati laboratories, Italy”, Proceedings of LINAC08, Victoria, BC, Canada, pp.618-620

[20] X.J. Wang and I. Ben-Zvi, “High-Brightness Electron Beam Diagnostics at the ATF”, Proceeding of BIW’96, AIP Conference Proceeding 390 (1996) 232-239.

[21] A.Cianchi et al., “High brightness electron beam emittance evolution measurements in an rf photoinjector”, Physical Review Special Topics Accelerator and Beams 11, 032801, 2008

[22] M.Ferrario et al., “Direct Measurement of the Double Emittance Minimum in the Beam Dynamics of the SPARC High-Brightness Photoinjector”, PRL 99, 234801 (2007)

[23] D. Filippetto, “A robust algorithm for beam emittance and trace space evolution reconstruction” SPARC Note SPARC/EBD-07/002.

[24] S. G. Anderson et al., ” Space-charge effects in high brightness electron beam emittance measurements”, PRST-AB, v 5, 014201 (2002)

[25] R. Thurman-Keup et al., ” Transverse emittance and phase space program developed for use at the Fermilab A0 photoinjector”, Proceedings of 2011 Particle Accelerator Conference, New York, NY, USA, MOP226

[26] S. Wojcicki, K.Friedel, „Systematical error of the measurement of electron beam emittance“,Vacuum, vol.51, Nr. 2, pp 113-118, 1998

[27] M.P. Stockli et al., "Self-consistent, unbiased exclusion methods of emittance analysis", Proceedings of the 2003 Particle Accelerator Conference, pp.527-529

[28] P. Castro, " Monte Carlo simulation of emittance measurements at TTF2" , DESY Technical Note 03 - 03 , 2003

[29] C. Limborg et al., "A modified quadscan technique for emittance measurement of space charge dominated beams", Proceedings of. PAC 2003, pp 2667 – 2669

[30] Mini Workshop on "Characterization of High Brightness Beams", DESY Zeuthen 2008.

[31] A. Murokh et al., "Limitations on measuring a transverse profile of ultradense electron beams with scintillators", Proceedings of the 2001 Particle Accelerator Conference, Chicago, pp.1333-1335

[32] A. Murokh et al., Proceedings of the 2nd ICFA Advanced Accelerator Workshop, 564-580 (2000)

[33] A.H. Lumpkin et al., Nucl. Instr. and Meth. A 429, 336-340 (1999)

[34] S.Rimjaem et al., "Comparison of different radiators used to measure the transverse characteristics of low energy electron beams at PITZ", DIPAC2011, TUPD54

[35] A. C. Kak and Malcolm Slaney, Principles of Computerized Tomographic Imaging, IEEE Press, 1988.

[36] D. Stratakis et al, "Tomography as a diagnostic tool for phase space mapping of intense particle beam", PRSTAB, 9, 112801 (2006)

[37] C. B. McKee, P. G. O'Shea, J. M. J. Madey, "Phase space tomography of relativistic electron beams", NIM A, Volume 358, pp 264-267, 1995

[38] V. Yakimenko et al., "Electron beam phase-space measurement using a high-precision tomography technique", PRSTAB, vol.6, 122801 (2003)

[39] J. G. Power "SLIT SCATTERING EFFECTS IN A WELL ALIGNED PEPPER POT", Proceedings of the 2003 Particle Accelerator Conference, pp.2432-2435

[40] H. Zen et al., "Quantitative evaluation of transverse phase space tomography", Proceedings of the 27th International Free Electron Laser Conference, pp. 592-594

[41] C. Bal, E. Bravin, T. Lefevre et al. Scintillating Screens Study for LEIR-LHC Heavy Ion Beams // Proc. of DIPAC 2005. Lyon, France, 2005.

[42] K.A. Brown, D.M. Gassner, Crystalline Chromium Doped Aluminium Oxide (Ruby) Use as a Luminescent Screen for Proton Beams // Proc. of PAC 1999. New York, USA, 1999.

[43] C. Nantista, C. Adolphsen., R.L. Brown, et al. Beam Profile Monitors in the NLCTA // Proc. of PAC 1997. Vancouver, Canada, 1997.

[44] H. Hayano. "Wire scanners for small emittance beam measurement in ATF." arXiv preprint physics/0008084 (2000).

[45] J. Frisch, et al. Beam Measurements at LCLS. No. SLAC-PUB-15018. SLAC National Accelerator Lab., Menlo Park, CA (United States), 2012.

[46] D.V. Karlovets and A.P. Potylitsyn, JETP Lett. 2009, Volume 90, Number 5, Pages 326-331

[47] D. V. Karlovets, JETP, 2011, Volume 113, Number 1, Pages 27-45

[48] V. L. Ginzburg, and I. M. Frank. "Radiation of a uniformly moving electron due to its transition from one medium into another." Journal of Physics (USSR) 9 (1945): 353-362.

[49] A.P. Potylitsyn, et al. "Radiation from relativistic particles." Diffraction Radiation

from Relativistic Particles. Springer, Berlin, Heidelberg, 2010.

[50] P. Karataev, A. Aryshev, S. Boogert, D. Howell, N. Terunuma, and J. Urakawa Physical Review Letters 107 (2011) 174801

[51] A. Aryshev, R, Ainsworth, T. Aumeyr, et al, Sub-micron scale transverse electron beam size diagnostics methodology based on the analysis of optical transition radiation source distribution. Journal of Instrumentation, 15(01), P01020, (2020)

[52] T. Watanabe et al, "Overall comparison of subpicosecond electron beam diagnostics by the polychromator, the interferometer and the femtosecond streak camera", NIMA, 480 (2002) 315–327

[53] P. Emma, J. Frisch, P. Krejcik,"A Transverse RF Deflecting Structure for Bunch Length and Phase Space Diagnostics ", LCLS TN 00 12, 2000

[54] D. Alesini, "RF deflector based sub ps beam diagnostics: application to FEL and advanced accelerators", International Journal of Modern Physics A, 22, 3693 (2007)

[55] C.P. Welsch "Development of longitudinal beam profile diagnostics within DITANET", Proceedings of 2011 Particle Accelerator Conference, New York, NY, USA, MOP185

[56] M. Hüning et al., "Observation of femtosecond bunch length using a transverse deflecting structure", Proceedings of the 27th International Free Electron Laser Conference, pp.538-541

[57] S. Zhang et al., "Temporal characterization of electron beam bunches with a fast streak camera at JLAB FEL facility", Proceedings of the 27th International Free Electron Laser Conference, pp.640-642.

[58] H.Loos et al., "Experimental studies of temporal electron beam shaping at the DUV-FEL accelerator", Proceedings of the 27th International Free Electron Laser Conference, pp.632-634.

[59] H.Loos, "Longitudinal diagnostics for short electron beam bunches", SLAC-PUB-14120

[60] S.J. Russel et al., " Subpicosecond Electron Bunch Diagnostic", LA-UR-2000-2135

[61] G. Berden et al., "Electo - Optic Technique with improved time resolution for real time, non destructive, single shot measurements of femtosecond electron bunch profiles, PRL v93, 11 (2004)

[62] B. Steffen, " Electro - optic time profile monitors for femtosecond electron bunches at the soft x-ray free electron laser FLASH ", PRSTAB, 12, 032802 (2009)

[63] Robinson L.C. Physical principles of far-infrared radiation. Academic Press, New York., 1973.

[64] Blaney T. G. Radiation detection at submillimetre wavelengths. Journal of Physics E: Scientic Instruments, 11:856{881, 1978.

[65] Emmons R. B., Hawkins S. R., and Cuff K. F. Optical Engineering, 14:21{30, 1975.

[66] Gillett F. C, Dereniak E. L., and Joyce R. R. Optical Engineering, 16:544{550, 1977.

[67] Kruse P. W. Optical and Infrared Detectors, pages 5{69. Springer-Verlag, Berlin and New York., 1977. R. J. Keyes, ed.

[68] Blaney T.G. Signal-to-noise ratio and other characteristics of heterodyne radiation receivers. Space Science Reviews, 17:691{702, 1975.